Enhanced Activity of Integrated CO_2 Capture and Reduction to CH_4 under Pressurized Conditions toward Atmospheric CO_2 Utilization

Kosaka, Fumihiko; Liu, Yanyong; Chen, Shih Yuan; Mochizuki, Takehisa; Takagi, Hideyuki; Urakawa, Atsushi; Kuramoto, Koji

DOI
10.1021/acssuschemeng.0c07162

Publication date
2021

Document Version
Accepted author manuscript

Published in
ACS Sustainable Chemistry and Engineering

Enhanced Activity of Integrated CO_2 Capture and Reduction to CH_4 under Pressurized Conditions Towards Atmospheric CO_2 Utilization

*Fumihiko Kosaka[1], Yanyong Liu[1], Shih-Yuan Chen[1], Takehisa Mochizuki[1], Hideyuki Takagi[1], Atsushi Urakawa[2] and Koji Kuramoto[1,]**

*Corresponding author: Tel: +81-29-861-8076; E-mail: koji-kuramoto@aist.go.jp

[1]*National Institute of Advanced Industrial Science and Technology (AIST), 16-1 Onogawa, Tsukuba, Ibaraki 305-8569, Japan*

[2]*Catalysis Engineering, Department of Chemical Engineering, Delft University of Technology, Van der Maasweg 9, 2629 HZ Delft, the Netherlands.*

KEYWORDS: CO_2 capture, CO_2 utilization, CO_2 reduction, dual functional catalyst, direct air capture, methanation,

ABSTRACT

Direct conversion of dilute CO_2 contained in power plant or industrial exhaust gas and the atmosphere into high-concentration hydrocarbons without a need of separate CO_2 capture and purification processes is one of the awaited technologies in envisioned low-carbon societies. In this study, we investigated the performance of integrated CO_2 capture and reduction to CH_4 over Ni-based dual functional catalysts promoted with Na, K and Ca. Ni/Na-γ-Al_2O_3 exhibited the highest activity for integrated CO_2 (5% CO_2) capture and reduction, achieving high CO_2 conversion (>96%) and CH_4 selectivity (>93%). In addition, very low concentration CO_2 (100 ppm CO_2) was successfully converted to 11.5% CH_4 at the peak point (>1000 times higher concentration than that of the supplied CO_2) over Ni/Na-γ-Al_2O_3. The Ni-based dual functional catalyst exhibited a high CO_2 conversion exceeding 90%, even when 20%O_2 was present during CO_2 capture. Furthermore, an increased operation pressure had positive impacts on both CO_2 capture and CH_4 formation, and these advantageous effects were also observed when CO_2 concentration was at the level of atmospheric CO_2 (100–400 ppm). As pressure increased from 0.1 to 0.9 MPa, CH_4 production capacity with 400 ppm CO_2 was enhanced from 111 to 160 μmol g_{cat}^{-1}. The approach in combination with the efficient catalyst shows encouraging promises for CO_2 utilization, enabling direct air capture-conversion to value-added chemicals.

INTRODUCTION

The aim to establish a low-carbon society has inspired the development of new technologies allowing one to reduce CO_2 emissions and improve energy efficiency by capturing CO_2 contained in power plant/industrial exhaust gas or even in the atmosphere and converting it into useful fuels and chemicals.[1–5] Such carbon capture and utilization processes (CCU) can be made even greener when coupled with reduction by H_2 produced by large-scale electrolysis of water using surplus or renewable source–derived electricity.[3,6,7] For example, CO_2 can be hydrogenated to form CH_4 according to the well-known Sabatier reaction (Eq. 1).[7–10]

$$CO_2 + 4H_2 \rightarrow CH_4 + 2H_2O \quad (1)$$

CO_2 methanation has attracted much attention as a means of effective CO_2/H_2 utilization and has been implemented in several pilot plants, e.g., Audi e-gas has been running a 6-MW demonstration plant since 2013.[6] In a conventional CCU process, flue gas with a low CO_2 content is passed through a CO_2 capture and separation unit to afford a CO_2-rich (~100%) feedstock suitable for subsequent utilization processes such as hydrogenation.[1] CO_2 can be separated from flue gas by absorption, physisorption, or gas separation membranes using amines, aqueous hydroxides, alkali carbonates, metal−organic frameworks, zeolites, and carbon-based materials as capture agents.[11–17] Despite the efforts made to improve the efficiency and energy cost of CO_2 capture and separation technologies,[11–17] CO_2 capture and separation from flue gas remains energy-consuming and costly, e.g., much thermal energy is consumed during CO_2 desorption.[18]

In the past years, the need to decrease the energy cost and increase the efficiency of CO_2

utilization has inspired the development of technologies allowing CO_2 contained in power plant/industrial exhaust gas or even in the atmosphere to be directly converted into high-concentration hydrocarbons or syngas without a separate CO_2 capture and separation process (Figure 1a).[19–37] These technologies convert dilute CO_2 directly into high concentrations of hydrocarbons in a single process. Such single-process methods are denoted as CO_2 capture and reduction (CCR) or integrated CO_2 capture and conversion (ICCC) (Figure 1b).

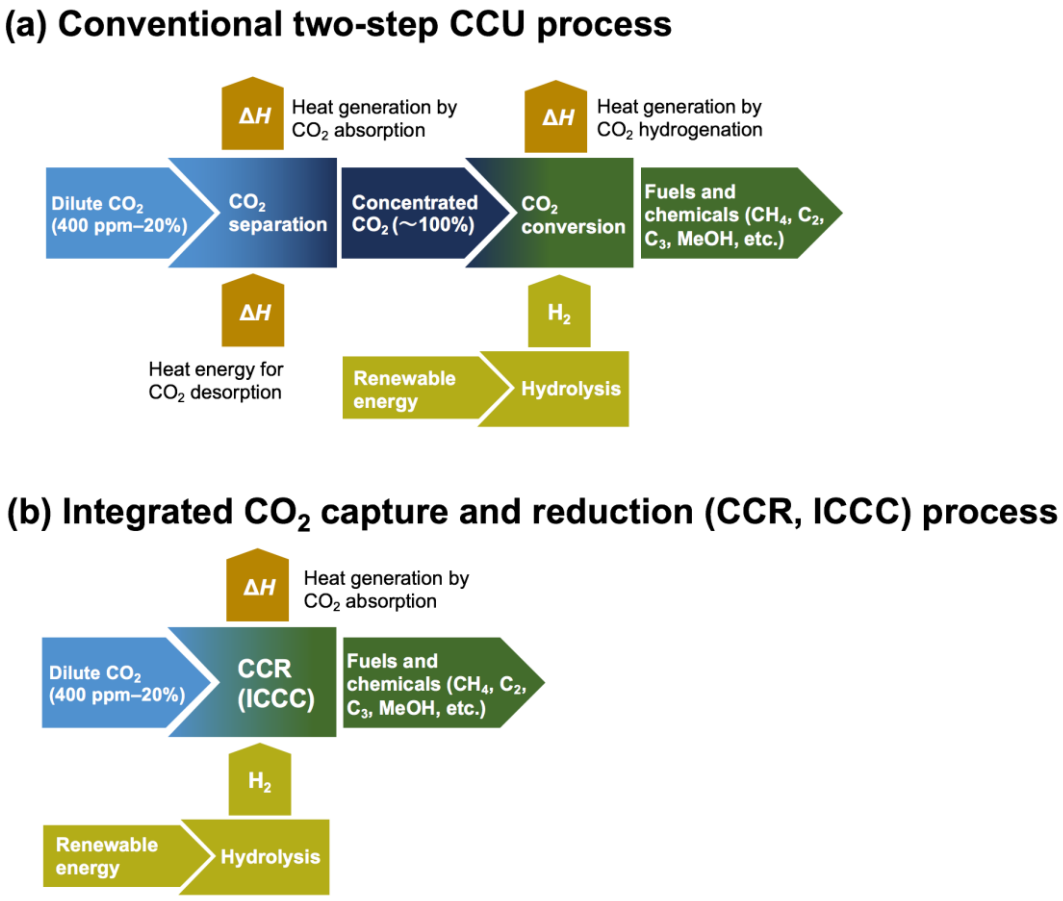

Figure 1. Conceptual diagram of (a) a conventional two-step CCU process and (b) an integrated process for the direct capture and reduction of dilute CO_2 into hydrocarbons over dual-functional catalysts.

The integrated CO_2 capture and conversion technology follows two reaction steps for CO_2 methanation as exemplified by the use of fluidized bed reactors as shown in Figure 2 and Eqs. 2–3. Below, alkaline/alkaline-earth metal oxides and carbonates are shown as representative material for CO_2 capture and formed after the capture, respectively. They can be different such as hydroxides and formates depending on the choice of constituting materials of catalyst[28].

Step 1 (CO_2 absorption): $A_nO + CO_2 \rightarrow A_nCO_3$ (A = Li, Na, K, Ca, Mg; n = 1 or 2) (2)

Step 2 (methanation of captured CO_2): $A_nCO_3 + 4H_2 \rightarrow A_nO + CH_4 + 2H_2O$ (3)

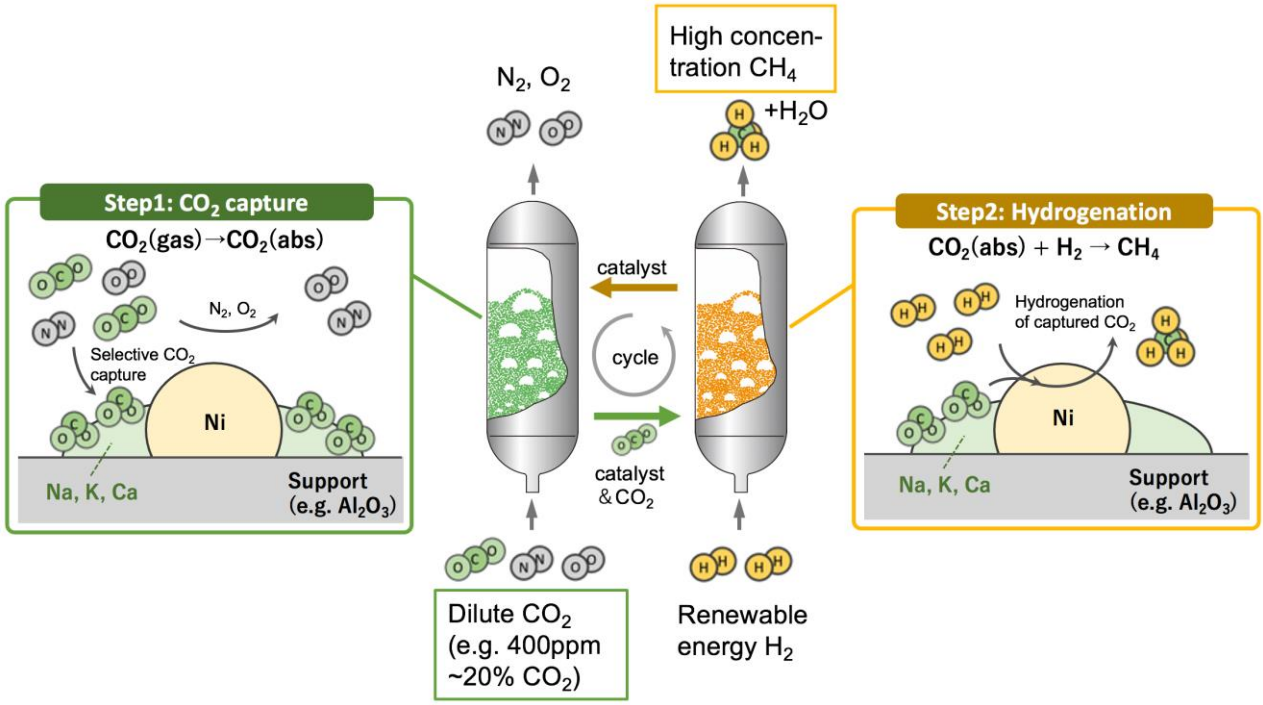

Figure 2. Conceptual diagram of the integrated process for the direct capture of dilute CO_2 into hydrocarbons over dual-functional catalysts using the circulating fluidized-bed reactor.

In step 1, CO_2 is selectively captured as alkali/alkaline earth metal carbonates inside/on the catalysts, while other gases such as N_2 and O_2 pass through (Eq. 2). In step 2, the catalyst is exposed to H_2 to convert the captured CO_2 into hydrocarbons such as CH_4 (Eq. 3). In the CO_2 reduction reactor (step 2), CO_2 desorption and CO_2 methanation reactions proceed simultaneously. CO_2 desorption is an endothermic reaction, while CO_2 methanation is exothermic. Therefore, the two reactions can be balanced in a single reactor in the CCR process by selecting the appropriate CO_2 absorber and reaction conditions. Large amounts of heat energy, that are otherwise required for conventional CO_2 separation and purification processes, are not needed in this process (Figure S1 and Table S1). Therefore, the CCR process can enhance the efficiency of the CCU process, although detailed quantitative discussions based on process simulations are necessary in the future.

In the CCR process, catalysts need to possess activity for both CO_2 capture and CO_2 reduction and are therefore called dual-functional catalysts. The concept of dual-functional catalysts was proposed in 2015 by Farrauto's group, who used Ru- and Ca-promoted γ-Al_2O_3 for the capture of 5 vol% CO_2 and its reduction by H_2 in a fixed-bed reactor at 320 °C.[23] The authors observed the formation of CH_4 upon switching from CO_2-containing gas to H_2 and thus demonstrated that a dual-functional catalyst can capture dilute CO_2 and directly convert it into CH_4.[23] Since then, the group has carried out other pioneering research, developing dual-functional catalysts with Ru, Rh, and Ni as active metal species and Na, K, and Mg as CO_2-absorbing components. [21,25,31,33,35,37] At the same period, Urakawa's group reported Fe- and Cu-based dual-functional catalysts directly converting dilute CO_2 into concentrated syngas.[19,28] FeCrCu/K/MgO-Al_2O_3 successfully absorbed 5–10% CO_2

and converted it into CO with a high selectivity of 90–96% in an H_2 atmosphere at 450–550 °C.[19] The excellent functionality was retained even when O_2 and H_2O vapor were present in the CO_2-containing gas stream[19]. Furthermore, they carried out space- and time-resolved *operando* diffuse reflectance infrared Fourier transform spectroscopy (DRIFTS), X-ray absorption spectroscopy (XAS) and X-ray diffraction (XRD) studies to elucidate the detailed reaction mechanism of CO_2 capture and reduction[28]. Regarding the utilization of very low CO_2 levels (e.g., atmospheric CO_2 levels of 400 ppm), Veselovskaya et al. reported a direct air capture and methanation process using separately allocated fixed-bed reactors containing a K-based CO_2 capture solid sorbent and methanation catalysts[26,30,36]. However, the future deployment of simpler CO_2 capture and reduction processes using fluidized-bed reactors (Figure 2) requires catalysts with dual functionality.

In this study, we developed Ni-based dual-functional catalysts and studied the effects of operating conditions on direct CO_2 capture and reduction to CH_4 using a fixed-bed reactor. As a well-known CO_2 methanation catalyst, Ni has an advantage over other active metals because of its relatively high natural abundance. Bermejo-López et al. investigated the optimization of active metal (Ni) content in dual-functional catalysts and realized a minor improvement (from 150 to 186 μmol g_{cat}^{-1} for Ni-Na_2CO_3/Al_2O_3) by catalyst composition tuning.[34] Obviously, the current challenges is how to enhance CO_2 capture capacity and CH_4 selectivity. Previous bifunctional catalytic CO_2 capture and reduction has been carried out at ambient pressure. Herein, we report significant improvements in these, facilitated by elevated reaction pressures (up to 0.9 MPa) besides tuning an appropriate catalyst composition. This approach is even able to efficiently capture 100-

400 ppm CO_2 and selectively convert it to CH_4. In addition, we report on the CO_2 capture and reduction performance of the Ni-based catalyst in the presence of O_2 during the CO_2 capture period.

EXPERIMENTAL

Preparation of Ni/(Na, K, Ca)/Al_2O_3 and Ni/Al_2O_3 catalysts

γ-Al_2O_3 (sample code: JRC-ALO-5, 74–125 μm) was supplied by the Catalysis Society of Japan (Japan Reference Catalysts). Na, K, Ca, and Ni precursors (Na_2CO_3, K_2CO_3, $Ca(NO_3)_2 \cdot 4H_2O$, and $Ni(NO_3)_2 \cdot 6H_2O$, respectively) were purchased from Fujifilm Wako Pure Chemical, Japan. γ-Al_2O_3 was impregnated with an aqueous solution (50 mL) containing Na, K, and Ca precursors, dried at 110 °C overnight, and calcined in air at 550 °C for 4 h. The alkali carbonate loading was maintained at 15 wt% against γ-Al_2O_3. The Na-, K-, and Ca-modified γ-Al_2O_3 was impregnated with an aqueous Ni precursor solution (50 mL) as described above, with the Ni loading maintained at 10 wt% against modified γ-Al_2O_3. As a result, Ni/Na-γ-Al_2O_3, Ni/K-γ-Al_2O_3, and Ni/Ca-γ-Al_2O_3 dual-functional catalysts were obtained. Ni/γ-Al_2O_3 prepared by incipient impregnation of γ-Al_2O_3 (JRC-ALO-5) with an aqueous Ni precursor solution as described above was used as a reference catalyst.

Catalyst Characterization

Wide-angle XRD patterns were recorded for 2θ = 10–80° on a Rigaku SmartLab SE diffractometer at 40 keV and 50 mA using a step size of 0.02° and a scan rate of 2 s per step. Cu K_α radiation (λ = 1.5418 Å) was used as the X-ray source. N_2 adsorption-desorption isotherms were recorded at −196 °C using a Belsorp max instrument for samples outgassed at 150 °C in high vacuum (<10^{-5} Torr). Specific surface area was calculated by the Brunauer-Emmett-Teller (BET) method at P/P_0 = 0.05–0.25. Pore volume was obtained by accumulation up to P/P_0 = 0.95. Pore size distribution was

analyzed by a non-linear density functional theory (NLDFT) method using a desorption branch. Temperature-programmed reduction (TPR) and temperature-programmed desorption (TPD) experiments were performed on a Belcat II instrument equipped with a thermal conductivity detector (TCD) and a BELMass mass spectrometer. Prior to H_2-TPR, the dried samples (~100 mg) were finely packed in a quartz tube and purged with a G1-grade standard of 5.05 vol% H_2/Ar at a flow rate of 15 mL min^{-1} at 50 °C until the TCD and MS signals were stable. Downstream composition was monitored by mass spectrometry and calibrated using standard gases. To enable comparison, the signals were normalized by sample weight. H_2-TPR-MS profiles were recorded at 50–950 °C and calibrated using a G1-grade standard gas of 1 vol% H_2/Ar. Prior to CO_2-TPD-MS measurements, the samples were reduced at 500 °C in a flow of H_2 (50 mL min^{-1}) for 1 h. For CO_2 chemisorption, a standard gas of 5 vol% CO_2/Ar was passed through the reduced samples at 50 °C for 30 min. Physically adsorbed CO_2 was purged by an Ar flow (50 mL min^{-1}) until the TCD and MS signals were stable. For to the Ar-TPD-MS measurement, the fresh samples were in situ reduced at 500 °C by a H_2 flow (50 mL min^{-1}) for 1 h, followed by purging with an Ar flow (50 mL min^{-1}) and cooling to 0 °C. Then, the hydrogen species remained on the reduced samples were gradually desorbed by heating and their amounts were monitored by the Ar-TPD-MS method.

CO_2 capture and reduction to CH_4 in a fixed-bed reactor

Figure S2 shows the experimental setup used for the integrated process of direct CO_2 capture and reduction into CH_4. Gas flow was automatically controlled using a gas supply system with mass

flow controllers (HM1000, HEMMI) and monitored by a non-dispersive infrared (NDIR) gas analyzer (VA-5000, HORIBA). Each catalyst (1 or 3 g) including the active components and the support was packed in a stainless-steel reactor (I.D.: 9 mm, catalyst bed height: ca. 20 mm), assembled in an electric furnace, and reduced at 500 °C in H_2 for 1 h at atmospheric pressure before the integrated process. Reaction temperature was monitored by placing a thermocouple in a 1/8-inch SUS tube inserted into the reaction tube. The integrated process consisted of the following steps: (i) CO_2 capture for 10 s–100 min, (ii) 5 min N_2 purging to remove unreacted CO_2, and (iii) reduction of the chemically captured CO_2 with H_2 for 5 min. Steps (i), (ii), and (iii) were performed using 0.01–13 vol% CO_2/N_2 (or 0.04 vol% CO_2/20%O_2/80%N_2), N_2, and H_2 as feed gases, respectively. The CO_2 capture and reduction cycle (steps (i–iii)) was repeated five times at 450 °C after H_2-pretreatment at 500 °C, with the results of the first cycle presented below and the results of the five cycles presented in Figure S3 and Figure S4. During operation, the temperature was maintained at 450 °C and the total gas flow rate was 50–500 NmL min^{-1}. Reaction pressure was varied from 0.1 to 0.9 MPa. The composition of the exhaust gas at the outlet was qualitatively and quantitatively analyzed using a BELMass mass spectrometer and an NDIR gas analyzer, respectively. The CH_4 formation (q_{CH_4}), CO formation (q_{CO}), and CO_2 capture (C_{CO_2}) capacities, as well as the CO_2 conversion (X_{CO2}), the selectivity for CH_4 or CO (S_i, i = CH_4 or CO), and the CO_2 capture efficiency (η_{CO_2}) were quantified using Eqs. 4–9, respectively.

$$q_{CH_4}\ [\mu mol\ g^{-1}] = \frac{1}{W}\int_{t_{H_2,\,in}}^{t_{H_2,\,out}} F_{CH_4}(t)dt, \quad (4)$$

$$q_{CO}\ [\mu mol\ g^{-1}] = \frac{1}{W}\int_{t_{H_2,\,in}}^{t_{H_2,\,out}} F_{CO,\,out}(t)dt, \quad (5)$$

$$C_{CO_2}\ [\mu mol\ g^{-1}] = \frac{1}{W}\int_{t_{H_2,\,in}}^{t_{H_2,\,out}}\left\{F_{CH_4,out}(t) + F_{CO,\,out}(t) + F_{CO_2,out}(t)\right\}dt, \quad (6)$$

$$X_{CO_2} = \frac{q_{CH_4} + q_{CO}}{C_{CO_2}}, \quad (7)$$

$$S_i = \frac{q_i}{q_{CH_4} + q_{CO}}, \quad (8)$$

$$\eta_{CO_2} = \frac{\int_{t_{H_2,\,in}}^{t_{H_2,\,out}}\left\{F_{CH_4,out}(t) + F_{CO,\,out}(t) + F_{CO_2,out}(t)\right\}dt}{F_{CO_2,in} \times t_{CO_2}} \quad (9)$$

where W, $F_{CH_4,out}$, $F_{CO_2,out}$, $F_{CO,out}$, $F_{CO_2,in}$, t_{CO_2}, $t_{H_2,\,in}$, and $t_{H_2,\,in}$ are the catalyst weight, the molar flow rates of CH_4, CO_2, and CO in the outlet gas, the molar flow rate of CO_2 in the inlet gas, the CO_2 supply period, the time of starting H_2 supply, and the time of ending H_2 supply, respectively.

RESULTS AND DISCUSSION

Screening of catalysts under atmospheric pressure

Figure 3 shows the performance of the integrated CO_2 capture and reduction process over dual functional catalysts (Ni/Na-γ-Al_2O_3, Ni/K-γ-Al_2O_3, and Ni/Ca-γ-Al_2O_3) examined at 450 °C under atmospheric pressure, in comparison to a reference catalyst (Ni/Al_2O_3). As aforementioned, this process can be divided into three steps: (i) chemical capture of CO_2 over Ni/Na-γ-Al_2O_3 corresponding to Eqs. (10)–(12),

$$Na_2O + CO_2 \rightarrow Na_2CO_3, \quad (10)$$

$$2NaOH + CO_2 \rightarrow Na_2CO_3 + H_2O, \quad (11)$$

$$NaOH + CO_2 \rightarrow NaHCO_3, \quad (12)$$

(ii) purging with N_2 for 5 min to eliminate gaseous and weakly sorbed CO_2, and (iii) hydrogenation

of the captured CO_2 in the H_2 flow (Eqs. (1), (13) and (14)).

$$CO_2 + H_2 \rightarrow CO + H_2O \quad (13)$$

$$CO + 3H_2 \rightarrow CH_4 + H_2O \quad (14)$$

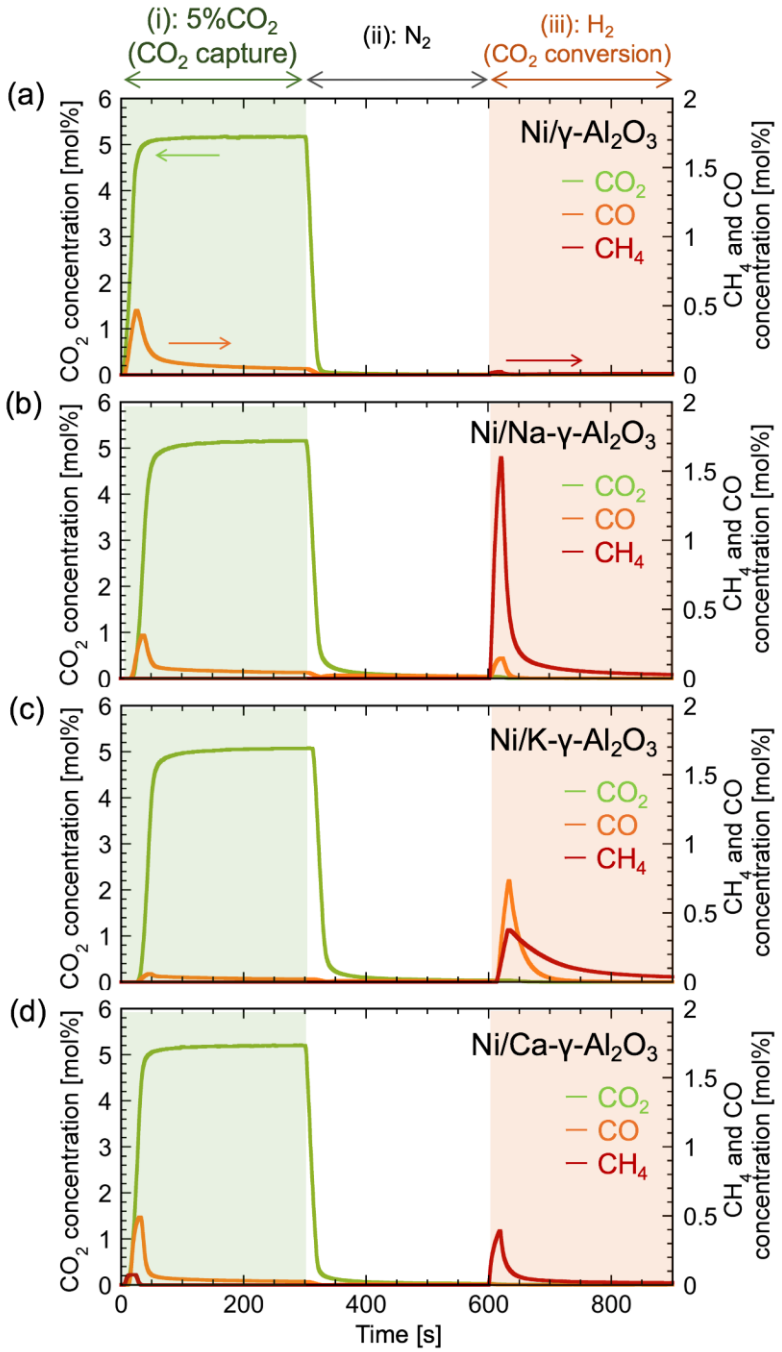

Figure 3. Performances of (a) Ni/γ-Al_2O_3, (b) Ni/Na-γ-Al_2O_3, (c) Ni/K-γ-Al_2O_3, and (d) Ni/Ca-γ-Al_2O_3 for integrated CO_2 capture and reduction into CH_4 at 450 °C and atmospheric pressure compared to Ni/Al_2O_3 as a reference catalyst. The gas flow (total flow rate = 500 mL min^{-1}) was stepwise switched from 5% CO_2 in N_2 to N_2 (at 300 s) and H_2 (at 600 s). Catalyst weight: 1g.

In Eqs. (10)-(12), sodium oxide and hydroxide were assumed as the CO_2 capture components and formation of sodium carbonate and bicarbonate was assumed as resulting components although the actual chemical states of captured CO_2 need to be verified[38–40]. In step (i), a small amount of CO was formed (Figure 3), possibly through the reduction of CO_2 by surface-adsorbed hydrogen (Eq. 15), particularly in the cases of Ni/γ-Al_2O_3 and Ni/Ca-γ-Al_2O_3.

$$2Ni\text{-}H_{ad} + CO_2 \rightarrow 2Ni + CO + H_2O, \quad (15)$$

In step (ii), a fast decrease in CO_2 content due to the N_2 purge was observed for Ni/γ-Al_2O_3 and Ni/Ca-γ-Al_2O_3. Delayed CO_2 content decay was observed for Ni/Na-γ-Al_2O_3 and Ni/K-γ-Al_2O_3, indicating that Na- and K- promotion enhanced the CO_2-catalyst interaction. In step (iii), negligible CH_4 formation was observed for conventional CH_4 methanation catalyst, Ni/γ-Al_2O_3, because of its small CO_2 capture capacity, which was ascribed to minor CO_2 adsorption (as opposed to absorption) during the CO_2 capture process. In contrast, large amounts of CH_4 and CO were produced over dual-functional catalysts. A large amount of CH_4 was formed over Ni/Na-γ-Al_2O_3, with a small amount of CO produced in the reduction phase. On the other hand, similar amounts of CO and CH_4 were generated over Ni/K-γ-Al_2O_3. Ni/Ca-γ-Al_2O_3 selectively afforded CH_4, albeit in a smaller amount than the Na-promoted catalyst. Although the CO_2 capture efficiency was <5% (Figure S5), we found that it could be improved, as detailed later. To focus on the effects of different catalysts and reaction conditions, such as the CO_2 concentration and pressure, sufficiently long CO_2 capture periods were generally used for the purpose of this study. It should be noted that the CH_4 concentration in the

outlet gas can be enhanced by increasing the ratio of the catalyst weight to the gas flow rate, as shown in Figure S12, and as described in previous literature[29], in which >60% CH_4 was obtained when employing a relatively large catalyst amount and a slow gas flow rate. In this study, a relatively high gas flow rate of 500 mL min^{-1} was generally used to improve the response of the gas analysis for the unsteady-state reaction, and to focus on the effects of the catalyst and reaction conditions (i.e., the pressure and CO_2 concentration).

Figure 4 quantifies CH_4 and CO formed in step (iii) and the amount of captured CO_2 based on Eqs. 4–6. The CO_2 capture and CH_4 formation capacities of Ni/γ-Al_2O_3 equaled 12.7 and 10.6 μmol g_{cat}^{-1}, respectively. In the case of Ni/Na-γ-Al_2O_3, the respective values (209 and 186 μmol g_{cat}^{-1}) were one order of magnitude higher, and a small amount of CO was also formed (13.8 μmol g_{cat}^{-1}). The selectivity for CH_4 reached 93%. Although the CO_2 capture capacity of Ni/K-γ-Al_2O_3 exceeded that of Ni/Na-γ-Al_2O_3, the CH_4 selectivity of the former was as low as 61% because of the formation of large amounts of CO. This finding demonstrates that the hydrogenation ability and selectivity of Ni are affected by the type of promoter used for CO_2 capture, which agrees with the previous literature where potassium on Ni catalysts enhances CO selectivity.[41] Ni/Ca-γ-Al_2O_3 was ineffective for capturing large amounts of CO_2, possibly because of the high stability of $CaCO_3$.[42] CO_2 release from $CaCO_3$ generally requires a high temperature of about 700°C, which is incompatible with the temperature range of CO_2 methanation.[42] Considering the above results, we mainly focused on the characterization and performance of Ni/Na-γ-Al_2O_3 under pressurized conditions.

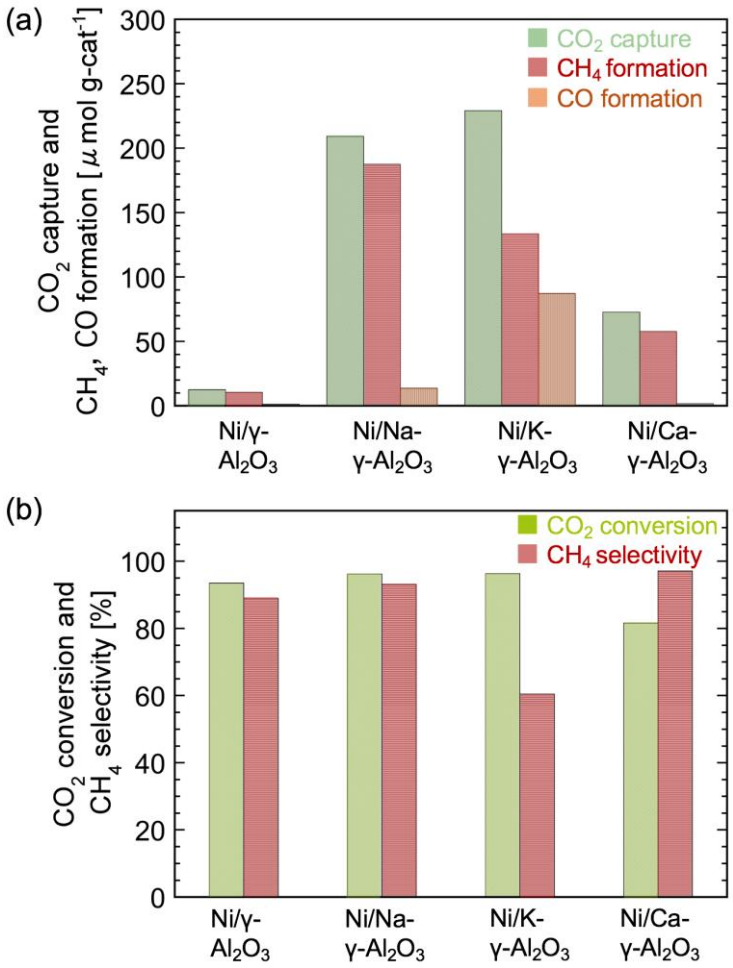

Figure 4. (a) CO/CH_4 production capacities and CO_2 capture capacities of Ni/Na-γ-Al_2O_3, Ni/K-γ-Al_2O_3, Ni/Ca-γ-Al_2O_3, and Ni/Al_2O_3 at 450 °C and atmospheric pressure and (b) corresponding CO_2 conversion (X_{CO2}) and CH_4 selectivity (S_{CH4}).

Characterization

The structural properties of Ni/Na-γ-Al_2O_3 and Ni/γ-Al_2O_3 were examined by wide-angle XRD, N_2 adsorption-desorption, H_2-TPR, Ar-TPD, and CO_2-TPD (Figures S6–S10). Figure S6 shows that no Ni species were detected in Ni/γ-Al_2O_3, indicating that Ni species were well dispersed on the γ-

Al_2O_3 framework. In contrast, the XRD pattern of fresh Ni/Na-γ-Al_2O_3 featured a weak peak at 2θ = 29.2° corresponding to the (200) plane of Na_2CO_3 and a series of NiO peaks. The NiO crystallite size was calculated as 25.3 nm by the Scherrer equation using the width at half height of the NiO (111) peak. Figure S7 shows the N_2 adsorption-desorption isotherms of as-prepared and reduced (at 500 °C) Ni/γ-Al_2O_3 and Ni/Na-γ-Al_2O_3 as well as the corresponding pore size distributions. All samples featured type-IV isotherms with an H_1 hysteresis loop associated with the mesoporous structure of γ-Al_2O_3.

The reducibility and basicity of Ni/Na-γ-Al_2O_3 were examined by H_2-TPR and CO_2-TPD, respectively (Figures S8 and S9). For Ni/Na-γ-Al_2O_3, NiO reduction was observed at lower temperatures (~500 °C, denoted as β') than for Ni/γ-Al_2O_3. This behavior suggested that the reduction of NiO was facilitated by the presence of Na, presumably because of the weak metal-support interaction of NiO and the Na-γ-Al_2O_3 surface. Figure S9 shows that the desorption of CO_2 from Ni/γ-Al_2O_3 was observed at 50–300 °C, with the corresponding peak centered at ~135 °C. The CO_2 uptake of this reference catalyst was determined as 0.12 mmol g^{-1}. In contrast, Ni/Na-γ-Al_2O_3 featured two strong signals centered at 166 and 630 °C, which were ascribed to the desorption of chemisorbed CO_2 and the thermal decomposition of Na_2CO_3, respectively. The CO_2 uptake of this catalyst (1.10 mmol g^{-1}) significantly exceeded that of the reference. Thus, the co-existence of Ni and Na was concluded to increase the number of catalytic sites for CO_2 chemisorption.

To elcidate the CO formation mechanism during the CO_2 capture step, we carried out the temperature-programmed desorption of the reduced catalysts in the Ar atmosphere (Figure S10).

The Ar-TPD-MS data can be employed to estimate the amount of hydrogen species adsorbed on the reduced samples. The results show that the amount of hydrogen adsorbed on the reduced catalysts is in the order of Ni/γ-Al_2O_3 > Ni/Na-γ-Al_2O_3 > Ni/Ca-γ-Al_2O_3 to Ni/K-γ-Al_2O_3, which is the same as the order of CO formation amount during the CO_2 capture step (Figure 3). It can be concluded based on these trends that the formation of the CO during the CO_2 capture step is related to the hydrogenation of CO_2 by the hydrogen adsorbed on the reduced catalysts.

Feasibility study of integrated CO_2 capture and reduction over Ni/Na-γ-Al_2O_3

Figure 5 shows the effect of the CO_2 capture period (10–60 s) on the integrated CO_2 capture and reduction performance over Ni/Na-Al_2O_3. When the CO_2 (13% CO_2) supply period was <30 seconds, the CO_2 concentration in the outlet gas was particularly low, and the majority of the supplied CO_2 was captured in the catalyst. Figure S13 shows the effect of the CO_2 supply period on the CO_2 capture efficiency, the CO_2 conversion, and the CH_4 selectivity. More specifically, the CO_2 capture efficiency was high when the CO_2 supply period was appropriate, and the efficiency decreased when the CO_2 supply period was too long due to the fact that the CO_2 capture capacity of the catalyst was saturated. Furthermore, it was found that the CO_2 conversion and CH_4 selectivity were improved when the hydrogenation of CO_2 was carried out, under the condition that the CO_2 absorption capacity of the catalyst was not saturated. These results may suggest that strongly-absorbed CO_2 exists in the early stages, while weakly-absorbed CO_2 exists in the near-saturation stages, and that these different CO_2 species may exhibit different activities for hydrogenation. In

addition, Figure 6 shows the gas concentration in the outlet when 100 ppm CO_2 was supplied at a rate of 500 mL min^{-1} for 1 h, followed by a supply of 50 mL min^{-1} of H_2, and using a Ni/Na-Al_2O_3 catalyst (3 g). In this case, 100 ppm CO_2 was successfully converted to 11.5% CH_4 at the peak point (>1000 times higher concentration than that of the supplied CO_2). These results indicate that the approach employed herein can efficiently convert dilute CO_2 into highly concentrated hydrocarbons without the requirement for CO_2 separation and purification.

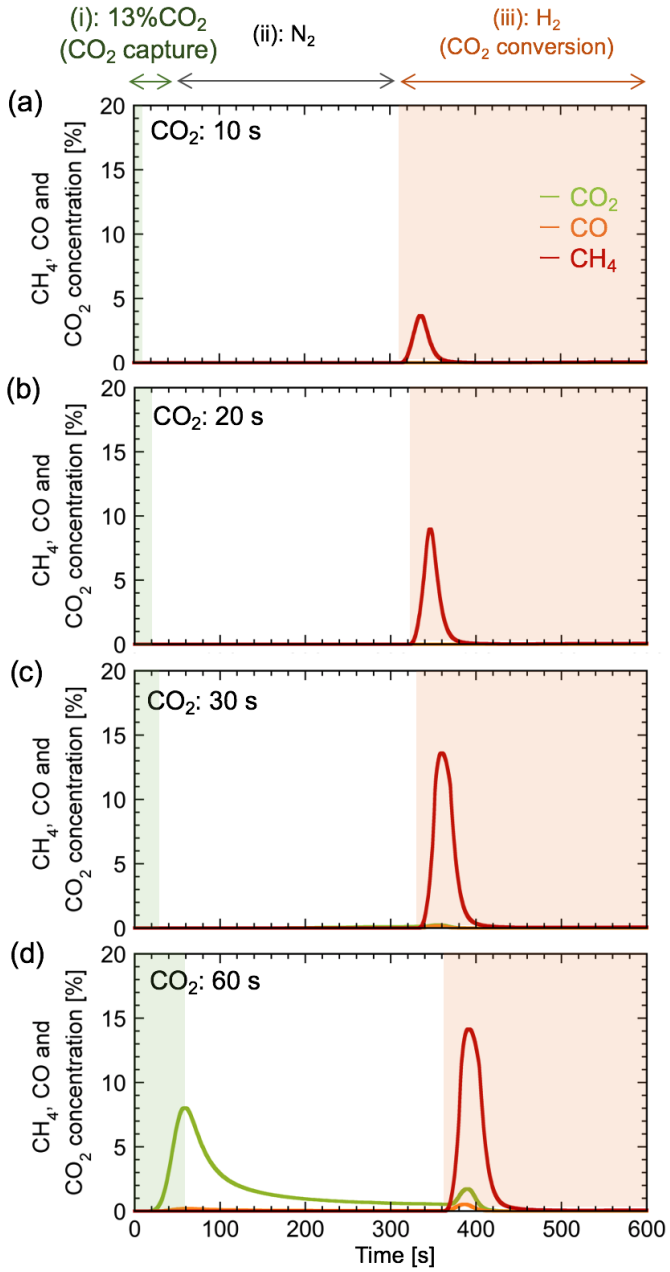

Figure 5. Effect of CO_2 capture period (10–60 s) on the integrated CO_2 capture and reduction into CH_4 over Ni/Na-γ-Al_2O_3 under atmospheric pressure. 3 g of catalyst was used, and the gas flow (total flow rate = 50 mL min^{-1}) was switched stepwise from 13% CO_2 in N_2 to N_2 and H_2.

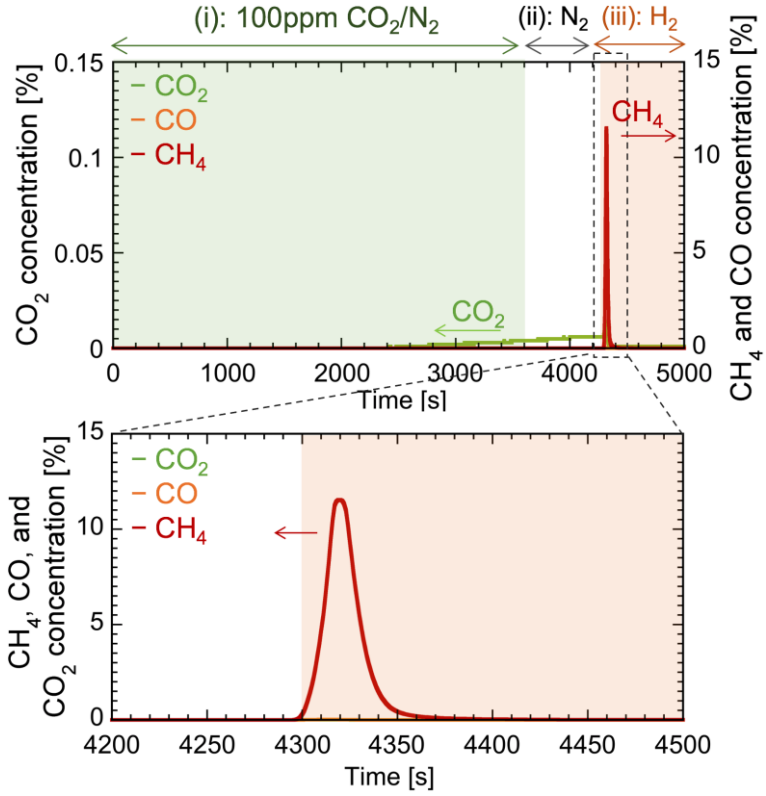

Figure 6. Evolution of product contents during 100 ppm CO_2 capture and reduction over Ni/Na-γ-Al_2O_3 at atmospheric pressure. The CO_2 capture period lasted for 1 h. 3 g of catalyst was used and the gas flow was switched stepwise from 100 ppm CO_2 in N_2 (total flow rate = 500 mL min^{-1}) to N_2 (500 mL min^{-1}) and H_2 (50 mL min^{-1}).

We investigated the CO_2 capture and reduction performance of the Ni/Na-Al_2O_3 in the presence of O_2 during the CO_2 capture period for atmospheric CO_2 utilization. Figure 7 shows the effect of O_2 during the CO_2 capture period on the CO_2 capture and reduction performance on Ni/Na-Al_2O_3. Although unreacted CO_2 formation under H_2 atmosphere increased for 400 ppm CO_2/20%O_2 (Figure 7(e) and 7(f)), the CH_4 formation amount was comparably high and the CH_4 selectivity was over 90% (Figure 7(f)). This result differs from the previous literature[37] that points the limitations of Ni during CO_2 capture in an O_2-containing atmosphere. However, the relatively high temperature of 450 °C and the difference in catalyst preparation may have influenced the Ni reactivation rate in

the H_2 atmosphere and the O_2 tolerance of the catalyst. Subsequently, this may have resulted in high performance under O_2-containing conditions in this study. Figure S14 shows the five cycles of CO_2 capture and CO_2 reduction using 400 ppm CO_2/20% O_2. The high CH_4 formation activity in the first cycle was maintained during several cycles, and the degradation of the catalyst exposed to O_2 was comparable to the degradation of the catalyst with 5% CO_2/N_2 for CO_2 capture (Figure S3(b)).

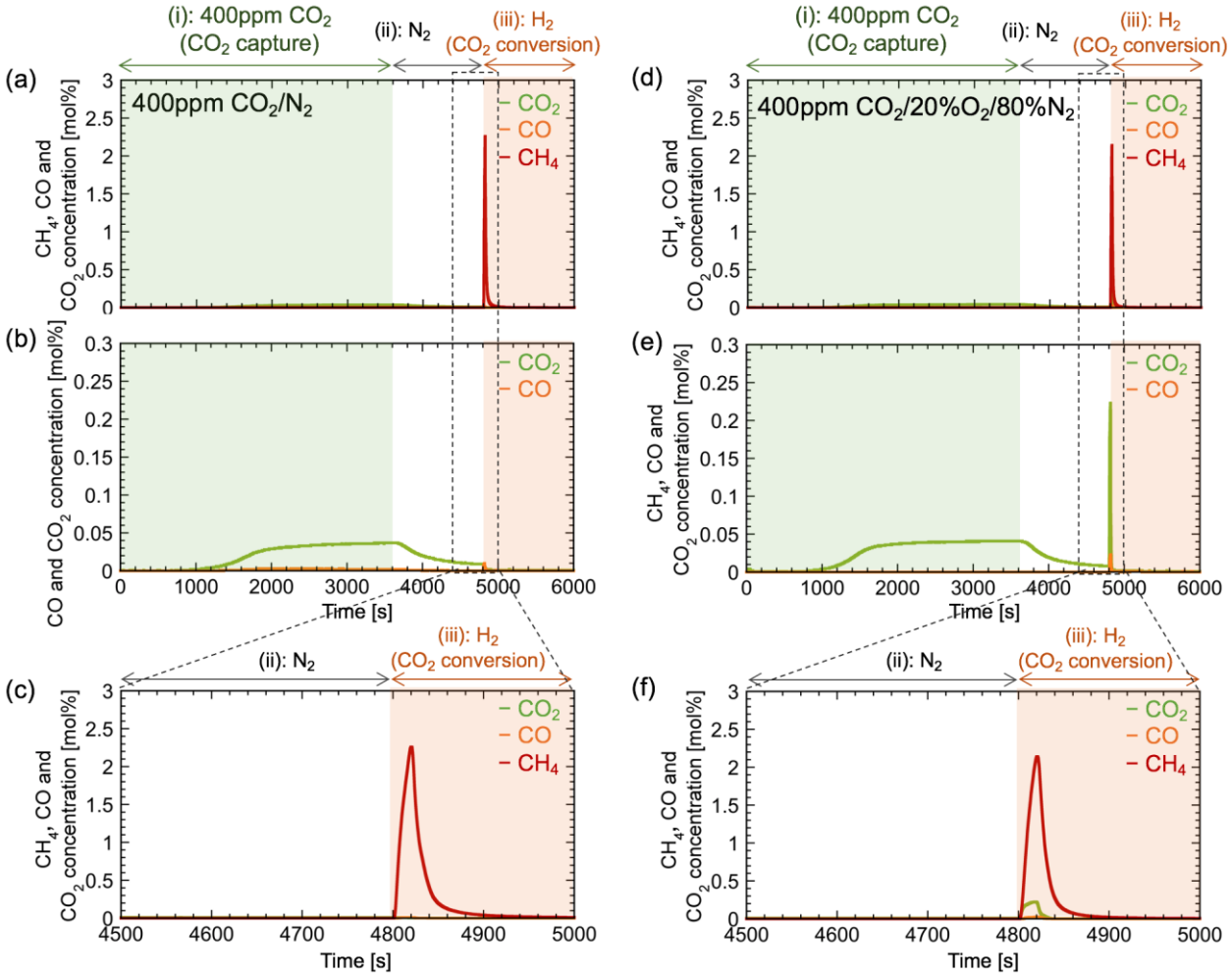

Figure 7. Effect of O_2 in CO_2 capture period on the integrated CO_2 capture and reduction into CH_4 over Ni-Na/γ-Al_2O_3 at 450 °C under atmospheric pressure. (a)-(c) 400 ppm CO_2/N_2 and (d)-(f) 400 ppm CO_2/20%O_2/80%N_2 for CO_2 capture. The gas flow (total flow rate = 200 mL min^{-1}) was stepwise switched from 400ppm CO_2 to N_2 (at 3600 s) and H_2 (at 4800 s). Catalyst weight: 1g.

Furthermore, we investigated the effect of CO_2 capture temperature in the presence of O_2 on the CH_4 formation performance. As shown in Figure 8, unreacted CO_2 release was almost negligible when the CO_2 capture temperature was lowered. In our future work, we consider using a circulating fluidized bed to realize a continuous process, as illustrated in Figure 2. Therefore, it is possible to operate the CO_2 capture reactor at a lower temperature compared to the CO_2 reduction reactor. The results suggest that a high CH_4 selectivity can be achieved and the oxidation of the earth's abundant Ni catalysts can be prevented by optimizing the CO_2 capture reactor temperature in the circulating fluidized bed for atmospheric CO_2 capture.

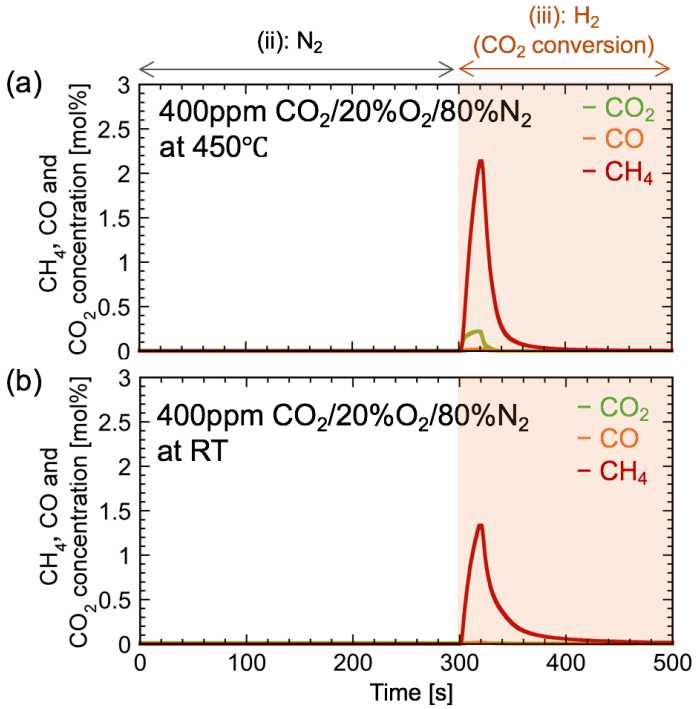

Figure 8. Effect of CO_2 capture temperature on the integrated CO_2 capture and reduction into CH_4 over Ni-Na/γ-Al_2O_3 under atmospheric pressure. CO_2 capture (400ppm CO_2/20%O_2/80%N_2) was performed at (a) 450 °C and (b) room temperature (20–25 °C), and then, reduction of the captured CO_2 by H_2 (300 s ~) was performed at 450 °C. Catalyst weight: 1g.

Enhanced capture and reduction of 5% CO_2 to CH_4 over Ni/Na-γ-Al_2O_3 under pressure

As shown in Figure 3, Ni/Na-γ-Al_2O_3 showed the highest activity for integrated CO_2 capture and reduction into CH_4 at atmospheric pressure. Therefore, this catalyst was used to examine the effects of pressure (0.1–0.9 MPa) and CO_2 content (5% and 100–400 ppm) relevant for direct air capture on the efficiency of CO_2 capture and reduction into CH_4. Figure 9 presents the effects of pressure, revealing that high pressure favored CH_4 formation. A transient and peaky response of the CH_4 signal was observed at all pressures, indicating that Ni/Na-γ-Al_2O_3 can provide a fast response during CO_2 reduction even under pressure.

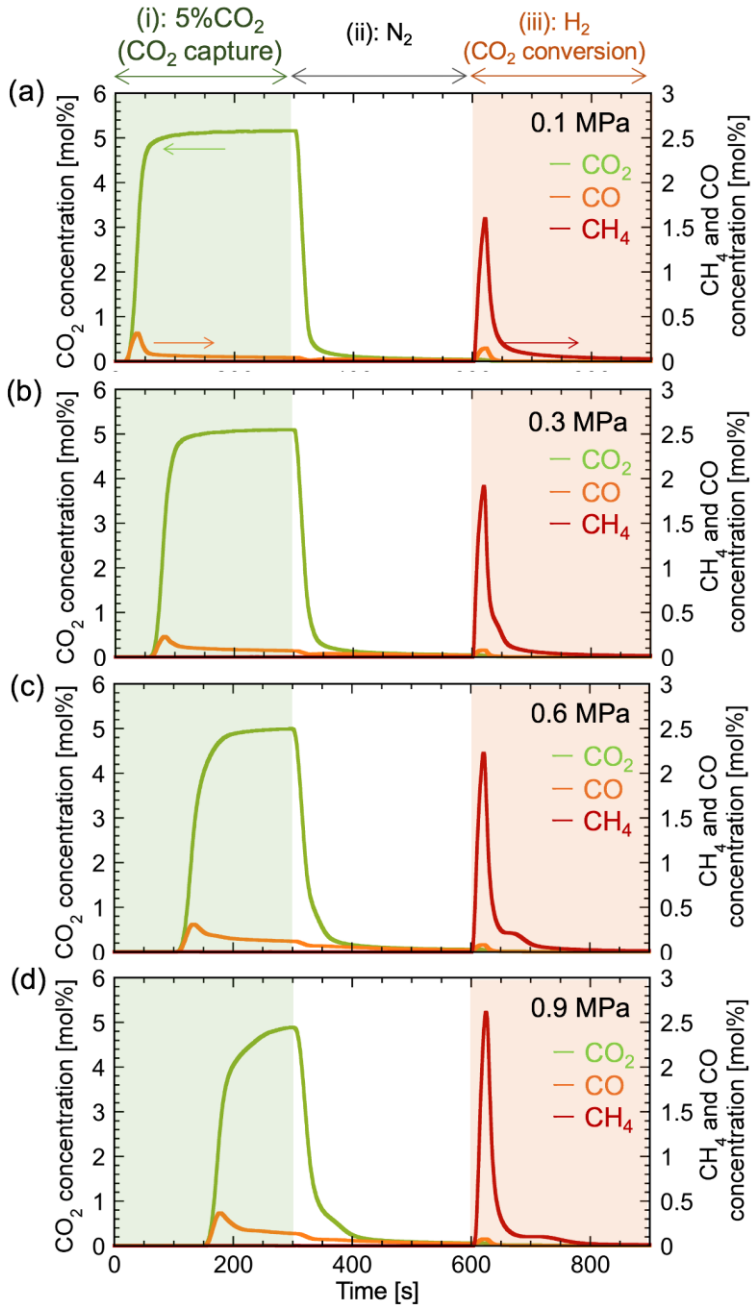

Figure 9. Effect of pressure (0.1–0.9 MPa) on the integrated CO_2 capture and reduction into CH_4 over Ni-Na/γ-Al_2O_3. The gas flow (total flow rate = 500 mL min^{-1}) was stepwise switched from 5% CO_2 in N_2 to N_2 (at 300 s) and H_2 (at 600 s). Catalyst weight: 1g.

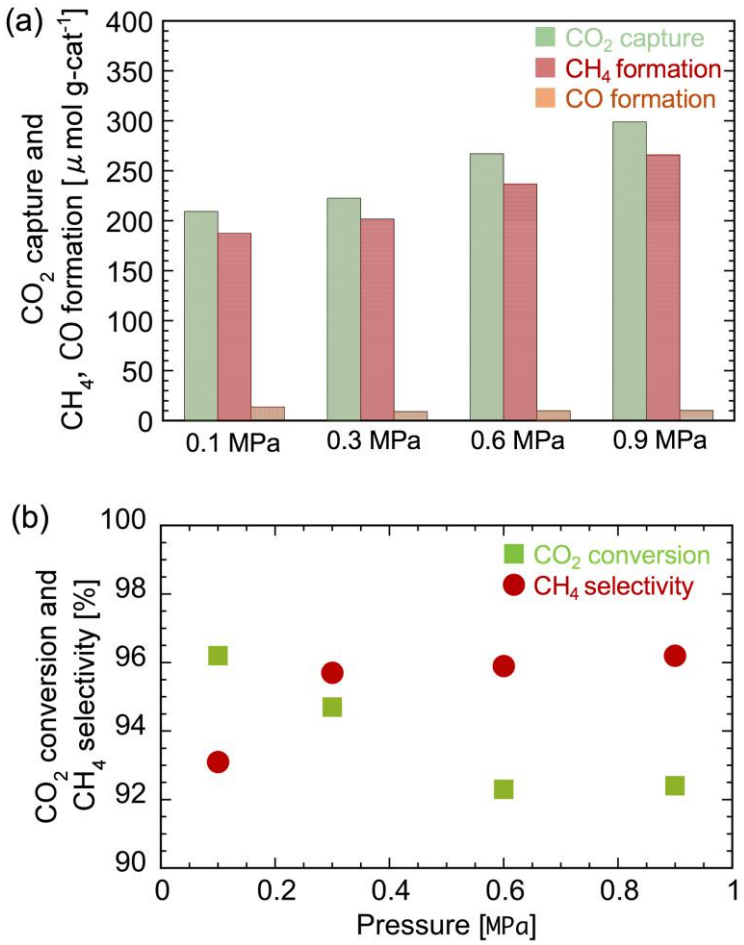

Figure 10. Effect of pressure on (a) CO_2 capture and CH_4 formation over Ni-Na/γ-Al_2O_3 and (b) corresponding CO_2 conversion (X_{CO2}) and CH_4 selectivity (S_{CH4}).

Figure 10(a) shows that high pressure increased the efficiencies of CO_2 capture and CO_2 reduction to CH_4 over Ni/Na-γ-Al_2O_3 while suppressing CO formation. Specifically, as pressure increased from ambient to 0.9 MPa, the CO_2 capture capacity increased from 209 to 299 μmol g_{cat}^{-1} (43% increase), while CH_4 formation capacity increased from 188 to 266 μmol g_{cat}^{-1} (41% increase). Figure 10(b) shows the effects of pressure on CO_2 conversion and CH_4 selectivity for Ni/Na-Al_2O_3. A high CO_2 conversion and a CH_4 selectivity of >92% were maintained despite the large CO_2 capture capacity under pressurized conditions. With increasing pressure, CH_4 selectivity increased

from 93 to 96%. These results suggest that high pressures positively affect the CO_2 capture and conversion performance of Ni/Na-Al_2O_3.

To investigate the influence of pressure on direct CO_2 capture and reduction, we examined the TPR of CO_2-loaded Ni/γ-Al_2O_3 and Ni/Na-γ-Al_2O_3 at 0.1–0.9 MPa. Prior to these experiments, the samples were reduced at 500 °C for 1 h, subjected to room-temperature CO_2 capture for 1 h, and then purged with a flow of H_2 for 30 min. TPR was performed from room temperature to 500 °C at a heating rate of 10 °C min^{-1}, and the outgas was quantitatively analyzed by the NDIR detector (Figure 11). For Ni/γ-Al_2O_3, the amounts of CO_2, CO, and CH_4 were small, which was ascribed to the small amount of physically and chemically adsorbed CO_2 on Ni/γ-Al_2O_3. Although CH_4 was observed at a relatively low temperature (~200 °C) because of the high methanation activity of Ni/γ-Al_2O_3, the effect of pressure on CO_2 capture capacity was also small for this catalyst. On the other hand, enhanced CO_2 desorption and CH_4/CO formation were observed for Ni/Na-γ-Al_2O_3. In addition, the signals of CO_2 and CH_4 (but not of CO) gained intensity with increasing pressure. High pressures favored the complete hydrogenation of CO_2 to CH_4 (Eq. 1) but hindered the hydrogenation of CO_2 to CO (Eq. 13) , especially at 0.9 MPa. This could be attributed to the advantageous pressure-dependency of the CO_2 methanation reaction (as predicted by Le Chatelier's principle). As pressure increased from atmospheric level to 0.9 MPa, no shift of the CO_2 desorption peak around 100 °C was observed, whereas the CH_4 formation peak shifted from 440 to 370 °C. This suggests that under pressurized conditions, the partial pressure of H_2 increases to accelerate the desorption of CO_2 and its conversion to CH_4.

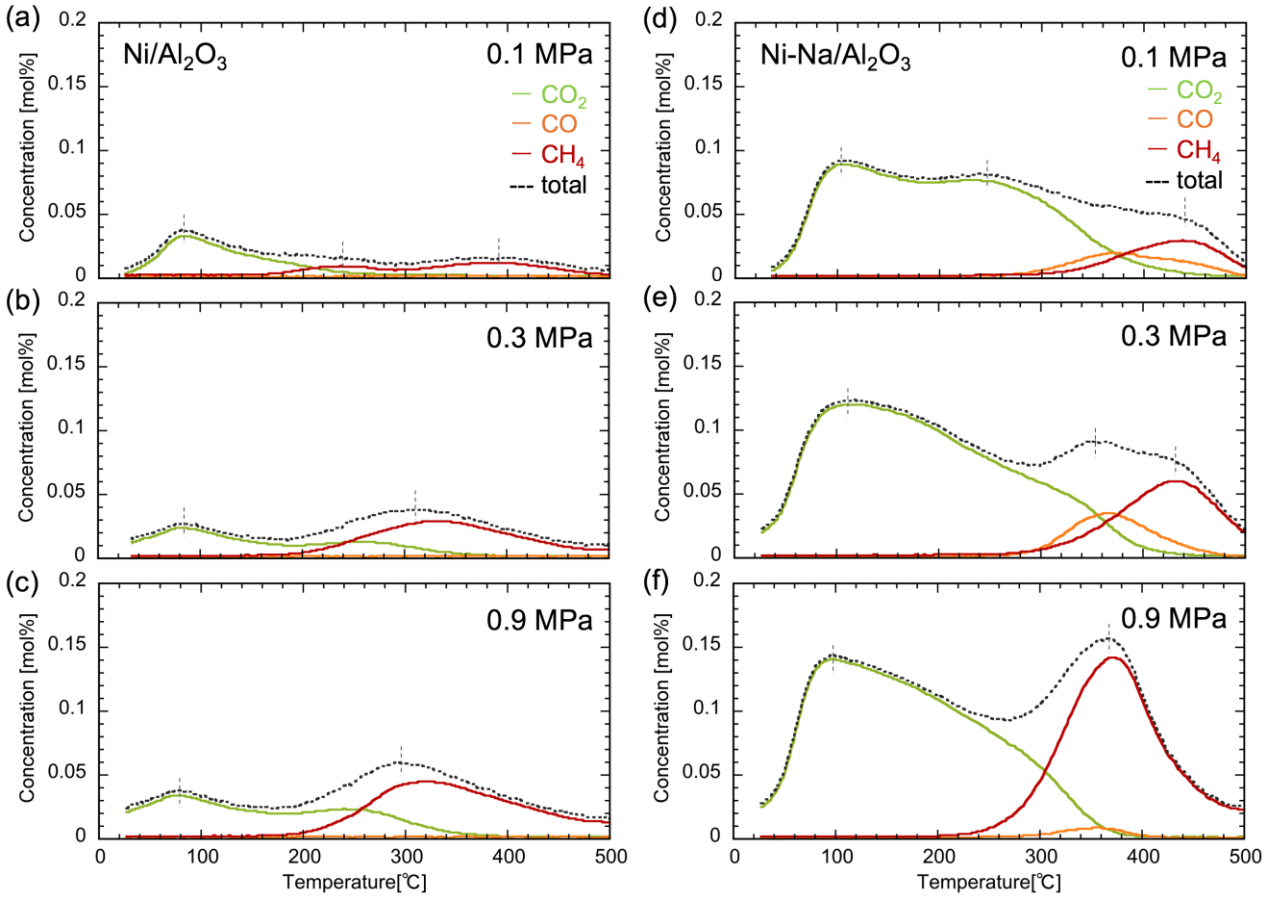

Figure 11. TPR profiles of CO_2-loaded catalysts [(a–c) Ni/γ-Al_2O_3 and (d–f) Ni-Na/γ-Al_2O_3] recorded at pressures of 0.1–0.9 MPa. Catalyst weight: 1g.

Enhanced capture and reduction of 100 and 400 ppm CO_2 to CH_4 over Ni/Na-γ-Al_2O_3 under pressure

Furthermore, we investigated the performance of Ni/Na-γ-Al_2O_3 for the integrated process at CO_2 levels relatively close to (400 ppm) and much lower than (100 ppm) that of atmospheric air (Figure 12).

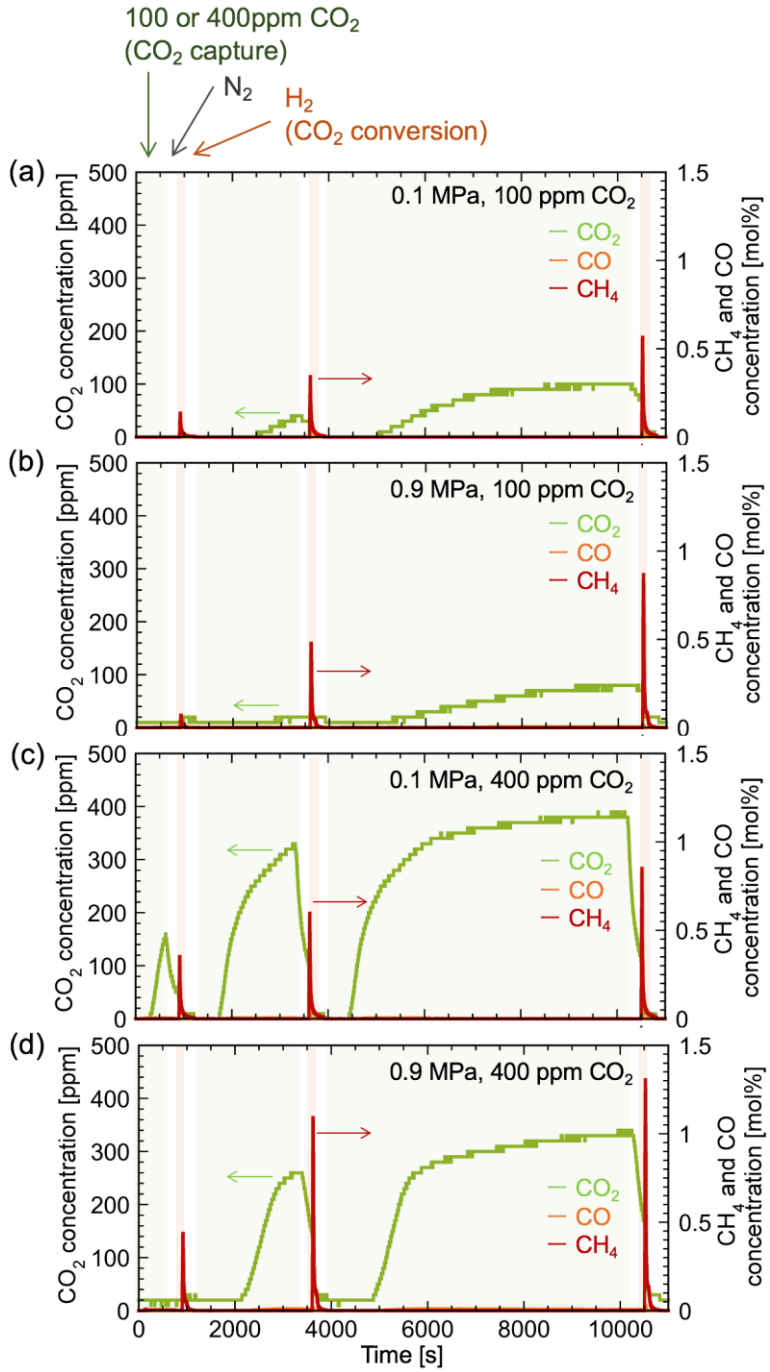

Figure 12. Evolution of product contents during dilute CO_2 capture and reduction on Ni-Na/γ-Al_2O_3 at variable pressures ((a), (c) 0.1 MPa atm and (b), (d) 0.9 MPa) and CO_2 levels ((a), (b)100 ppm and (c), (d) 400 ppm CO_2 diluted with N_2). The CO_2 capture period lasted for 10, 30, or 100 min, and the total flow rate equaled 500 mL min^{-1}. Catalyst weight: 1g.

As shown in Figure 12, elevated pressure promoted CH_4 formation. As described in the previous section, the CH_4 concentration in the outlet gas can be further improved for practical application by optimizing the gas flow rate. For both 100 and 400 ppm CO_2, the amounts of CH_4 formed at 0.9 MPa exceeded those observed at atmospheric pressure. In addition, CH_4 formation was promoted by extending the CO_2 capture period from 10 to 100 min, as also follows from enhanced CO_2 capture at higher pressures. In the case of 100 ppm CO_2 and 0.1 MPa (Figure 12(a)), CO_2 was observed in the outlet gas after 15 min of CO_2 supply, which indicated the concomitant saturation of Ni/Na-γ-Al_2O_3. On the other hand, saturation proceeded slowly at 0.9 MPa (Figure 12(b)). This result indicates that the CO_2 absorption capacity of the dual-functional catalyst increased with increasing pressure and, more importantly, the catalyst was able to efficiently capture CO_2 at low levels.

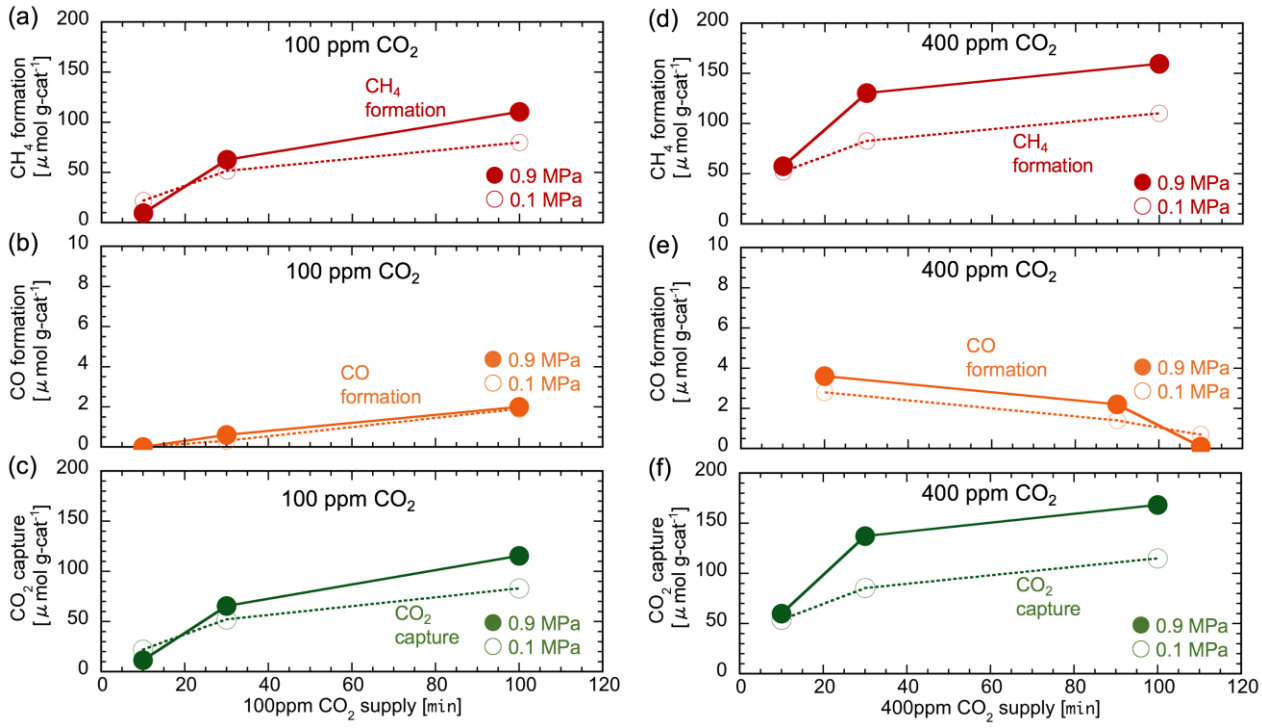

Figure 13. Effect of pressure on (a), (d) CH_4 formation, (b), (e) CO formation, and (c), (f) CO_2

capture performances with 100 ppm and 400 ppm CO_2 of Ni-Na/γ-Al_2O_3.

Figure 13 summarizes the effects of pressure on CH_4 formation, CO formation, and CO_2 capture performances. For Ni/Na-γ-Al_2O_3, the amounts of produced CH_4 and captured CO_2 increased with increasing pressure and CO_2 capture period. CO formation was insignificant, and CO_2 conversion and CH_4 selectivity exceeded 96% under all conditions. Figure S15 shows CO_2 capture efficiency for 100 and 400 ppm CO_2 capture and reduction. As indicated, a relatively high CO_2 capture efficiency was obtained when an appropriate CO_2 capture period was employed.

Table 1. Integrated CO_2 capture and reduction performances of Ni-based dual-functional catalysts reported previously and those described in the present work. All experiments were conducted in a fixed-bed reactor.

Catalyst	CO_2 concentration [%]	CO_2 capture [μmol g_{cat}^{-1}]	CH_4 formation [μmol g_{cat}^{-1}]	CO_2 conversion [%]	CH_4 selectivity [%]	Temperature [°C]	Pressure [MPa]	Ref.
Ni/K-γ-Al_2O_3	5% CO_2/N_2	229	134	96	61	450	0.1	This work
Ni/Ca-γ-Al_2O_3	5% CO_2/N_2	73	58	82	97	450	0.1	This work
Ni/Na-γ-Al_2O_3	5% CO_2/N_2	209	188	96	93	450	0.1	This work
	5% CO_2/N_2	299	266	92	96	450	0.9	This work
	400 ppm CO_2/N_2	168	159	97	98	450	0.9	This work
	100 ppm CO_2/N_2	116	111	98	98	450	0.9	This work
Ni-CaO/Al_2O_3	25% CO_2/Ar,	171	142	–	–	520	0.1	[34]
Ni-Na_2CO_3/Al_2O_3	25% CO_2/Ar,	215	186	–	–	400	0.1	[34]
Ni-Na_2O/Al_2O_3	7.5% CO_2/N_2	398	276	71	–	320	0.1	[37]
Ni-K/ZrO_2, Ni-La/ZrO_2	4.7% CO_2/He	–	–	51 32	98 99	350	0.1	[20]

Table 1 compares the integrated CO_2 capture and reduction performances of previously reported Ni-based dual functional catalysts and those described herein, revealing that pressure elevation increased the efficiency of 5% CO_2 capture by Ni/Na-γ-Al_2O_3 from 209 to 299 μmol g_{cat}^{-1}. Furthermore, for 400 and 100 ppm CO_2, pressurization allowed the amount of produced CH_4 to be increased to 159 and 111 μmol g_{cat}^{-1}, respectively. These values are higher than or comparable to those of previous studies of alkali- or alkaline-promoted Ni/γ-Al_2O_3 and Ni/ZrO_2 catalysts, which were examined by the relatively high concentration of the CO_2 mixture gas (4.7–25% CO_2) under atmospheric pressure. Thus, the investigated dual-functional catalysts could successfully capture CO_2 within a wide content range (100 ppm to 5%) and simultaneously convert it into CH_4 with very high CO_2 conversion and CH_4 selectivity. The results indicate that pressure significantly affects the activity of dual-functional catalysts for integrated CO_2 capture and reduction, suggesting that pressure elevation is an effective

way of improving the efficiency of CO_2 utilization.

CONCLUSIONS

Herein, we investigated the effects of pressure on the performance of Ni-based dual-functional catalysts for integrated CO_2 capture and reduction to CH_4. Specifically, Ni/Na-γ-Al_2O_3, Ni/K-γ-Al_2O_3, and Ni/Ca-γ-Al_2O_3 were prepared as dual-functional catalysts, and Ni/γ-Al_2O_3 was prepared as a reference catalyst. Among these catalysts, Ni/Na-γ-Al_2O_3 showed the highest activity for integrated CO_2 capture (5 vol% CO_2 absorption) and conversion into CH_4, achieving high CO_2 conversion (>96%) and CH_4 selectivity (>93%). It was found that the CO_2 capture efficiency was particularly high when an appropriate CO_2 supply period was employed. In addition, very low concentration CO_2 (100 ppm CO_2) was successfully converted to 11.5% CH_4 (>1000 times higher concentration than that of the supplied CO_2) over Ni/Na-γ-Al_2O_3. Furthermore, we investigated the CO_2 capture and reduction performance in the presence of O_2 during the CO_2 capture period for atmospheric CO_2 utilization. Although the formation of unreacted CO_2 under H_2 atmosphere increased slightly in the presence of O_2 during CO_2 capture, the amount of CH_4 formation was comparably high. Moreover, CO_2 conversion was over 90% on Ni/Na-Al_2O_3. By lowering the CO_2 capture temperature, unreacted CO_2 release was almost negligible and CH_4 selectivity was further improved. Both CO_2 capture and CH_4 formation were favored by high pressure, e.g., as pressure increased from 0.1 to 0.9 MPa, CO_2 capture capacity increased from 209 to 299 μmol g_{cat}^{-1}, while

CH_4 productivity increased from 188 to 266 μmol g_{cat}^{-1}. In addition, the effect of pressure on catalyst performance was also investigated at very low CO_2 levels of 100 and 400 ppm, and high pressure was found to positively affect both CO_2 capture and CH_4 formation. These results suggest that high pressure enhances the CO_2 absorption and CH_4 formation capacities of dual-functional catalysts and allows for efficient integrated CO_2 capture and reduction into CH_4 even at atmospheric levels of CO_2. The approach, in combination with the efficient catalyst, is promising for CO_2 utilization, thus enabling direct air capture-conversion to value-added chemicals.

AUTHOR INFORMATION

Corresponding Author

Koji Kuramoto, PhD

National Institute of Advanced Industrial Science and Technology (AIST), 16-1 Onogawa, Tsukuba, Ibaraki 305-8569, Japan

Tel: +81-; E-mail: koji-kuramoto@aist.go.jp

Author Contributions

The manuscript was written through contributions from all authors. All authors have approved the final version of the manuscript.

REFERENCES

(1) Koytsoumpa, E. I.; Bergins, C.; Kakaras, E. The CO_2 Economy: Review of CO_2 Capture and Reuse Technologies. *J. Supercrit. Fluids* **2018**, *132*, 3–16.

(2) Li, W.; Wang, H.; Jiang, X.; Zhu, J.; Liu, Z.; Guo, X. A Short Review of Recent Advances in CO2 Hydrogenation to Hydrocarbons over Heterogeneous Catalysts. *RSC Adv.* **2018**, *8*, 7651–7669.

(3) Götz, M.; Lefebvre, J.; Mörs, F.; McDaniel Koch, A.; Graf, F.; Bajohr, S.; Reimert, R.; Kolb, T. Renewable Power-to-Gas: A Technological and Economic Review. *Renew. Energy* **2016**, *85*, 1371–1390.

(4) Mota, F. M.; Kim, D. H. From CO_2 Methanation to Ambitious Long-Chain Hydrocarbons: Alternative Fuels Paving the Path to Sustainability. *Chem. Soc. Rev.* **2019**, *48*, 205–259.

(5) Rafiee, A.; Rajab Khalilpour, K.; Milani, D.; Panahi, M. Trends in CO_2 Conversion and Utilization: A Review from Process Systems Perspective. *J. Environ. Chem. Eng.* **2018**, *6*, 5771–5794.

(6) Wulf, C.; Linßen, J.; Zapp, P. Review of Power-to-Gas Projects in Europe. *Energy Procedia* **2018**, *155*, 367–378.

(7) Ghaib, K.; Fatima-Zahrae Ben-Fares. Power-to-Methane: A State-of-the-Art Review. *Renew. Sustain. Energy Rev.* **2018**, *81*, 433–446.

(8) Rönsch, S.; Schneider, J.; Matthischke, S.; Schlüter, M.; Götz, M.; Lefebvre, J.; Prabhakaran,

P.; Bajohr, S. Review on Methanation - From Fundamentals to Current Projects. *Fuel* **2016**, *166*, 276–296.

(9) Su, X.; Xu, J.; Liang, B.; Duan, H.; Hou, B.; Huang, Y. Catalytic Carbon Dioxide Hydrogenation to Methane : A Review of Recent Studies. *J. Energy Chem.* **2016**, *25*, 553–565.

(10) Aziz, M. A. A.; Jalil, A. A.; Triwahyono, S.; Ahmad, A. CO_2 Methanation over Heterogeneous Catalysts: Recent Progress and Future Prospects. *Green Chem.* **2015**, *17*, 2647–2663.

(11) Olajire, A. A. Synthesis Chemistry of Metal-Organic Frameworks for CO_2 Capture and Conversion for Sustainable Energy Future. *Renew. Sustain. Energy Rev.* **2018**, *92*, 570–607.

(12) Wang, J.; Huang, L.; Yang, R.; Zhang, Z.; Wu, J.; Gao, Y.; Wang, Q.; O'Hare, D.; Zhong, Z. Recent Advances in Solid Sorbents for CO_2 Capture and New Development Trends. *Energy Environ. Sci.* **2014**, *7*, 3478–3518.

(13) Sanz-Pérez, E. S.; Murdock, C. R.; Didas, S. A.; Jones, C. W. Direct Capture of CO_2 from Ambient Air. *Chemical Reviews*. 2016, 11840–11876.

(14) Yu, C. H.; Huang, C. H.; Tan, C. S. A Review of CO_2 Capture by Absorption and Adsorption. *Aerosol Air Qual. Res.* **2012**, *12*, 745–769.

(15) Kierzkowska, A. M.; Pacciani, R.; Müller, C. R. CaO-Based CO2 Sorbents: From Fundamentals to the Development of New, Highly Effective Materials. *ChemSusChem* **2013**, *6*, 1130–1148.

(16) Mondal, M. K.; Balsora, H. K.; Varshney, P. Progress and Trends in CO_2 Capture/Separation Technologies: A Review. *Energy* **2012**, *46*, 431–441.

(17) Brunetti, A.; Scura, F.; Barbieri, G.; Drioli, E. Membrane Technologies for CO_2 Separation. *J. Memb. Sci.* **2010**, *359*, 115–125.

(18) Rubin, E. S.; Davison, J. E.; Herzog, H. J. The Cost of CO_2 Capture and Storage. *Int. J. Greenh. Gas Control* **2015**, *40*, 378–400.

(19) Bobadilla, L. F.; Riesco-García, J. M.; Penelás-Pérez, G.; Urakawa, A. Enabling Continuous Capture and Catalytic Conversion of Flue Gas CO_2 to Syngas in One Process. *J. CO_2 Util.* **2016**, *14*, 106–111.

(20) Hu, L.; Urakawa, A. Continuous CO2 Capture and Reduction in One Process: CO_2 Methanation over Unpromoted and Promoted Ni/ZrO2. *J. CO_2 Util.* **2018**, *25*, 323–329.

(21) Zheng, Q.; Farrauto, R.; Chau Nguyen, A. Adsorption and Methanation of Flue Gas CO_2 with Dual Functional Catalytic Materials: A Parametric Study. *Industrial and Engineering Chemistry Research*. 2016, 6768–6776.

(22) Al-Mamoori, A.; Rownaghi, A. A.; Rezaei, F. Combined Capture and Utilization of CO_2 for Syngas Production over Dual-Function Materials. *ACS Sustainable Chemistry and Engineering*. 2018, 13551–13561.

(23) Duyar, M. S.; Treviño, M. A. A.; Farrauto, R. J. Dual Function Materials for CO_2 Capture and Conversion Using Renewable H_2. *Applied Catalysis B: Environmental*. 2015, 370–376.

(24) Sun, H.; Wang, J.; Zhao, J.; Shen, B.; Shi, J.; Huang, J.; Wu, C. Dual Functional Catalytic

Materials of Ni over Ce-Modified CaO Sorbents for Integrated CO_2 Capture and Conversion. *Appl. Catal. B Environ.* **2019**, *244*, 63–75.

(25) Duyar, M. S.; Wang, S.; Arellano-Treviño, M. A.; Farrauto, R. J. CO_2 Utilization with a Novel Dual Function Material (DFM) for Capture and Catalytic Conversion to Synthetic Natural Gas: An Update. *J. CO_2 Util.* **2016**, *15*, 65–71.

(26) Veselovskaya, J. V.; Parunin, P. D.; Netskina, O. V.; Okunev, A. G. A Novel Process for Renewable Methane Production: Combining Direct Air Capture by K_2CO_3/Alumina Sorbent with CO_2 Methanation over Ru/Alumina Catalyst. *Top. Catal.* **2018**, *61*, 1528–1536.

(27) Cimino, S.; Boccia, F.; Lisi, L. Effect of Alkali Promoters (Li, Na, K) on the Performance of Ru/Al_2O_3 Catalysts for CO_2 Capture and Hydrogenation to Methane. *J. CO_2 Util.* **2020**, *37*, 195–203.

(28) Hyakutake, T.; Van Beek, W.; Urakawa, A. Unravelling the Nature, Evolution and Spatial Gradients of Active Species and Active Sites in the Catalyst Bed of Unpromoted and K/Ba-Promoted Cu/Al_2O_3 during CO_2 Capture-Reduction. *J. Mater. Chem. A* **2016**, *4*, 6878–6885.

(29) Miguel, C. V.; Soria, M. A.; Mendes, A.; Madeira, L. M. A Sorptive Reactor for CO_2 Capture and Conversion to Renewable Methane. *Chem. Eng. J.* **2017**, *322*, 590–602.

(30) Veselovskaya, J. V.; Parunin, P. D.; Netskina, O. V.; Kibis, L. S.; Lysikov, A. I.; Okunev, A. G. Catalytic Methanation of Carbon Dioxide Captured from Ambient Air. *Energy* **2018**, *159*, 766–773.

(31) Wang, S.; Schrunk, E. T.; Mahajan, H.; Farrauto, R. J. The Role of Ruthenium in CO_2 Capture

and Catalytic Conversion to Fuel by Dual Function Materials (DFM). *Catalysts* **2017**, *7*, 1–13.

(32) Kim, S. M.; Abdala, P. M.; Broda, M.; Hosseini, D.; Copéret, C.; Müller, C. Integrated CO_2 Capture and Conversion as an Efficient Process for Fuels from Greenhouse Gases. *ACS Catalysis*. 2018, 2815–2823.

(33) Proaño, L.; Tello, E.; Arellano-Trevino, M. A.; Wang, S.; Farrauto, R. J.; Cobo, M. In-Situ DRIFTS Study of Two-Step CO_2 Capture and Catalytic Methanation over Ru,"Na_2O"/Al_2O_3 Dual Functional Material. *Appl. Surf. Sci.* **2019**, *479*, 25–30.

(34) Bermejo-López, A.; Pereda-Ayo, B.; González-Marcos, J. A.; González-Velasco, J. R. Ni Loading Effects on Dual Function Materials for Capture and In-Situ Conversion of CO_2 to CH_4 Using CaO or Na_2CO_3. *J. CO_2 Util.* **2019**, *34*, 576–587.

(35) Wang, S.; Farrauto, R. J.; Karp, S.; Jeon, J. H.; Schrunk, E. T. Parametric, Cyclic Aging and Characterization Studies for CO_2 Capture from Flue Gas and Catalytic Conversion to Synthetic Natural Gas Using a Dual Functional Material (DFM). *J. CO_2 Util.* **2018**, *27*, 390–397.

(36) Veselovskaya, J. V.; Parunin, P. D.; Okunev, A. G. Catalytic Process for Methane Production from Atmospheric Carbon Dioxide Utilizing Renewable Energy. *Catal. Today* **2017**, *298*, 117–123.

(37) Arellano-Treviño, M. A.; He, Z.; Libby, M. C.; Farrauto, R. J. Catalysts and Adsorbents for CO_2 Capture and Conversion with Dual Function Materials: Limitations of Ni-Containing

DFMs for Flue Gas Applications. *J. CO_2 Util.* **2019**, *31*, 143–151.

(38) Keturakis, C. J.; Ni, F.; Spicer, M.; Beaver, M. G.; Caram, H. S.; Wachs, I. E. Monitoring Solid Oxide CO_2 Capture Sorbents in Action. *ChemSusChem* **2014**, *7*, 3459–3466.

(39) Nikulshina, V.; Ayesa, N.; Gálvez, M. E.; Steinfeld, A. Feasibility of Na-Based Thermochemical Cycles for the Capture of CO_2 from Air-Thermodynamic and Thermogravimetric Analyses. *Chem. Eng. J.* **2008**, *140*, 62–70.

(40) Siriwardane, R. V.; Robinson, C.; Shen, M.; Simonyi, T. Novel Regenerable Sodium-Based Sorbents for CO_2 Capture at Warm Gas Temperatures. *Energy and Fuels* **2007**, *21*, 2088–2097.

(41) Campbell, T. K.; Falconer, J. L. Carbon Dioxide Hydrogenation on Potassium-Promoted Nickel Catalysts. *Appl. Catal.* **1989**, *50*, 189–197.

(42) Blamey, J.; Anthony, E. J.; Wang, J.; Fennell, P. S. The Calcium Looping Cycle for Large-Scale CO_2 Capture. *Prog. Energy Combust. Sci.* **2010**, *36*, 260–279.

Graphycal Abstract

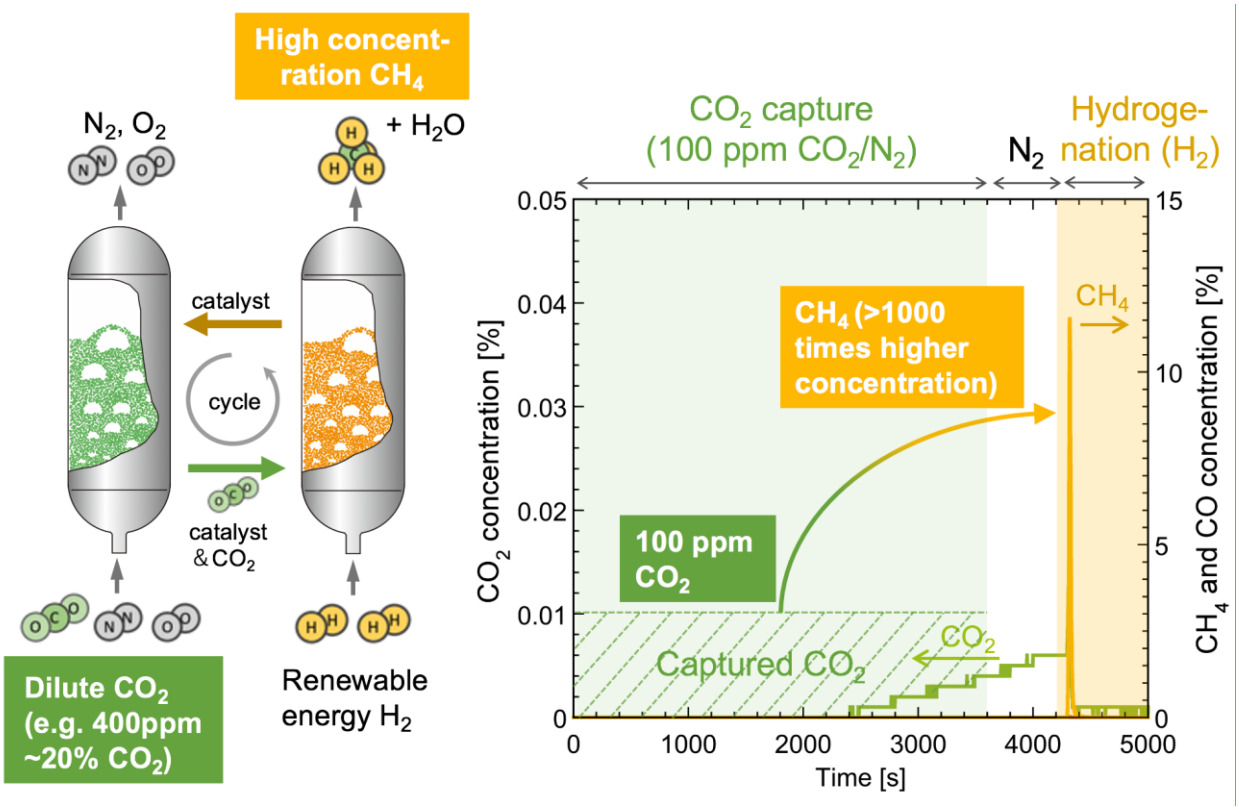

Synopsis: High pressure promoted the integrated capture and reduction (to CH_4) of dilute CO_2 over a Ni-based Al_2O_3-supported catalys